2 **Weaning Recovery** 3 Yihan Li¹, Chantal M. J. de Bakker^{1,2}, Xiaohan Lai³, Hongbo Zhao¹, Ashutosh Parajuli⁴, Wei-Ju 4 Tseng¹, Shaopeng Pei^{1,4}, Tan Meng¹, Rebecca Chung¹, Liyun Wang⁴, and X. Sherry Liu^{1*} 5 6 7 8 ¹ McKay Orthopaedic Research Laboratory, Department of Orthopaedic Surgery, Perelman 9 School of Medicine, University of Pennsylvania, Philadelphia, PA, United States 10 ² Department of Radiology, Cumming School of Medicine, McCaig Institute for Bone and Joint Health, University of Calgary, Calgary, Canada 11 ³ Division of Life Sciences and Medicine, University of Science and Technology of China, 12 13 Hefei, China ⁴ Center for Biomechanical Research, Department of Mechanical Engineering, University of 14 Delaware, Newark, DE, USA 15 16 17 18 19 *To whom correspondence should be addressed 20 X. Sherry Liu 21 McKay Orthopaedic Research Laboratory Department of Orthopaedic Surgery 22 23 University of Pennsylvania 332A Stemmler Hall, 3450 Hamilton Walk 24 25 Philadelphia, PA 19104, USA 26 Email: xiaoweil@pennmedicine.upenn.edu 27 Phone: 1-215-746-4668 28 29 30 **Conflict of Interest:** The authors declare that they have no conflict of interest. 31 32 33 Number of words in abstract: 261 34 5968 Number of words in manuscript: 35 Number of tables: 0 36 Number of figures: 6

Maternal Bone Adaptation to Mechanical Loading during Pregnancy, Lactation, and Post-

Abstract:

37

38

39

40

41

42

43

44

45

46

47

48

49

50

51

52

53

54

55

56

57

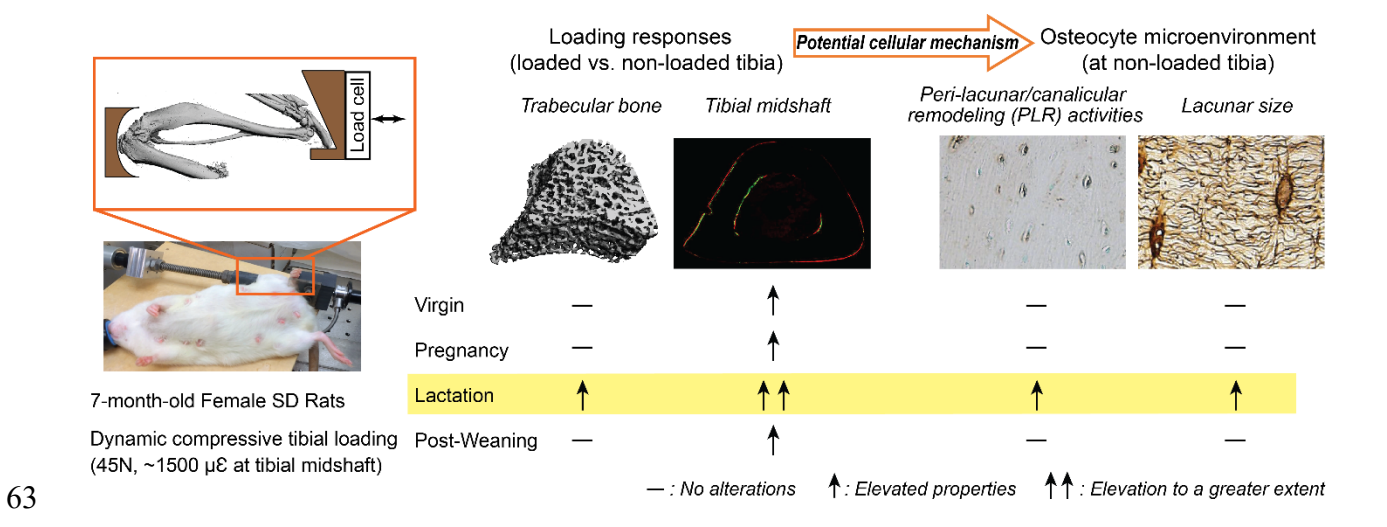
58

59

The maternal skeleton undergoes dramatic bone loss during pregnancy and lactation, and substantial bone recovery post-weaning. The structural adaptations of maternal bone during reproduction and lactation exert a better protection of the mechanical integrity at the critical load-bearing sites, suggesting the importance of physiological load-bearing in regulating reproduction-induced skeletal alterations. Although it is suggested that physical exercise during pregnancy and breastfeeding improves women's physical and psychological well-being, its effects on maternal bone health remain unclear. Therefore, the objective of this study was to investigate the maternal bone adaptations to external mechanical loading during pregnancy, lactation, and post-weaning recovery. By utilizing an *in vivo* dynamic tibial loading protocol in a rat model, we demonstrated an improved maternal cortical bone structure in response to dynamic loading at tibial midshaft, regardless of reproductive status. Notably, despite the minimal loading responses detected in the trabecular bone in virgins, the rat bone during lactation experienced enhanced mechano-responsiveness in both trabecular and cortical bone compartments when compared to rats at other reproductive stages or age-matched virgins. Furthermore, our study showed that the lactation-induced elevation in osteocyte peri-lacunar/canalicular remodeling (PLR) activities led to enlarged osteocyte lacunae. This may result in alterations in interstitial fluid flow-mediated mechanical stimulation on osteocytes and an elevation in solute transport through the lacunar-canalicular system (LCS) during high-frequency dynamic loading, thus enhancing mechano-responsiveness of maternal bone during lactation. Taken together, findings from this study provide important insights into the relationship between reproduction and lactation-induced skeletal changes and external mechanical loading, emphasizing the importance of weight-bearing exercise on maternal bone health during reproduction and postpartum.

- 60 **Keywords:** Maternal bone adaptation; Bone mechano-responsiveness; Reproduction; Lactation;
- Peri-lacunar/canalicular remodeling (PLR); Osteocyte mechanosensing

62 Graphic Abstract:



1. Introduction

64

65

66

67

68

69

70

71

72

73

74

75

76

77

78

79

80

81

82

83

84

85

86

During reproduction and lactation, the maternal skeleton serves as an important reservoir for minerals, notably calcium and phosphorus, which can be accessed to allow the body to support fetal/infant growth and maintain homeostasis [1]. In women, the resulting skeletal resorption can lead to 1-4% decline in areal bone mineral density (aBMD) during pregnancy [2-6], and 4-8% reduction in BMD during lactation [6-11]. More strikingly, rodent studies have shown that lactation can result in 20-80% reduction in bone mass due to higher calcium requirement by the larger litter size in mice and rats [1, 12, 13]. Following weaning, the maternal skeleton undergoes a remarkable anabolic phase, leading to substantial recovery of bone mass and bone microstructure [1, 14-17]. Intriguingly, the extent to which bone structure is recovered post-weaning is site-dependent. Clinical studies observed that the recovery of bone mass is greater in the spine than long bones [1, 6, 7, 18]. Recent clinical and rodent studies demonstrated that maternal bone undergoes substantial structural adaptation to maintain the mechanical integrity of the high load-bearing skeletal regions, e.g., trabecular compartment of the lumbar vertebrae and the cortical compartment of the long bone [18-25]. These findings suggested that physiological load-bearing may play an important role in regulating reproduction-induced skeletal alterations.

Despite the significant reduction in bone mass and mechanical properties, pregnancy- and lactation-associated fracture is uncommon [1]. Nevertheless, women with low bone mass or skeletal fragility prior to pregnancy may be predisposed to a higher risk of fractures. Given the importance of physiological load-bearing on regulating reproduction-induced skeletal changes, we asked the question: would external mechanical loading exert a protective and beneficial effect on bone health during reproduction, lactation, and post-weaning recovery? Although it is

suggested that physical exercise during pregnancy and breastfeeding benefits women's physical and psychological well-being [26], clinical investigations have reported variable results on the relationship between weight-bearing exercises and bone health during pregnancy and lactation. Some studies suggest that the physical activity is associated with a reduced extent of aBMD loss during pregnancy and lactation [27, 28], while others reported no benefits [29, 30]. An animal study using a bipedal stance model in rats found that weight-bearing exercise during pregnancy attenuated trabecular bone loss at the tibial metaphysis and increased cortical bone strength at the tibial diaphysis by the end of lactation [31]. Despite these previous data, further investigations are required to elucidate the detailed effects of mechanical loading on reproduction- and lactation-induced bone changes. Therefore, the first objective of this study was to investigate the maternal bone adaptations to external mechanical loading by utilizing an *in vivo* dynamic tibial loading protocol during pregnancy, lactation, and post-weaning recovery in a rat model. We hypothesized that external dynamic loading would attenuate the bone loss induced by pregnancy and lactation, and enhance the bone recovery post-weaning.

In addition, we also aimed to explore potential mechanisms through which the skeleton efficiently balances its metabolic and mechanical function during reproduction and lactation. As the long-lived primary mechanosensory cells in bone, the osteocytes likely play an important role in mediating skeletal mechano-responsiveness during reproduction and lactation. Osteocytes form an extensive cellular network through their numerous cell processes housed in the lacunar-canalicular system (LCS), an interconnected set of pores and channels embedded in the mineralized bone matrix. This LCS network allows nutrient supply, waste removal, and transport of signaling molecules [32, 33]. Moreover, loading-induced interstitial fluid flow inside the LCS transmits macroscopic mechanical stimuli to osteocytes through shear stress on the cell process

and fluid drag on the tethering elements that connect the cell processes with canalicular wall, triggering the release of various osteocytic signaling molecules that regulate mineral homeostasis [34]. LCS structure is thus a key determinant of fluid and solute transport that is essential for osteocyte signal transduction. Several studies in mice have demonstrated that, in various conditions, most notably during lactation, the LCS is modified through osteocyte perilacunar/canalicular remodeling (PLR) [35-41]. This lactation-induced PLR may alter the LCS porosity and the pericellular matrix (PCM) around osteocytes, thus affecting flow-mediated mechanosensing and diffusion/convection of nutrients and signaling molecules for osteocytes [13, 42]. Although the lactation-associated PLR has been demonstrated in mice, whether PLR occurs during lactation in rats still remains unclear. Therefore, the second objective of this study was to assess the effects of pregnancy, lactation, and post-weaning recovery on osteocyte microenvironment in a rat model. Based on the previous findings in mice, we hypothesized that osteocytes can actively remodel their peri-lacunar/canalicular bone matrix through PLR during lactation in rats, and this altered osteocyte microenvironment might be associated with altered mechano-responsiveness of post-partum bone.

2. Methods

110

111

112

113

114

115

116

117

118

119

120

121

122

123

124

125

126

127

128

129

130

131

132

2.1 Animal Protocol

All animal protocols were approved by the University of Pennsylvania's Institutional Animal Care and Use Committee. Female, Sprague Dawley rats were assigned to 4 groups (n=10-11/group): Pregnancy, Lactation, Post-Weaning, and Virgin. Different timing of mating was chosen for each group so that all rats reached the same age of 26 weeks when loading experiments started (Figure 1). All rats received 2 weeks of dynamic loading. Rats in the Pregnancy group received dynamic loading from day 3.8±2.2 to day 17.8±2.2 of pregnancy. To

confirm the success of the pregnancy, euthanasia was delayed until parturition (4.2 days after the end of dynamic loading). Rats in the Lactation group underwent pregnancy followed by 14 days of lactation (loading initiated from day 1 of lactation) before euthanasia. Rats in the Post-Weaning group underwent pregnancy, 21 days of lactation, and 14 days of post-weaning recovery (loading initiated from day 1 post-weaning) before euthanasia.

To ensure sufficient dietary calcium content, all rats were fed a high-calcium diet (LabDiet 5001 Rodent Diet; 0.95% Ca). All litters were normalized to 9 pups per mother within 24 hours of birth for consistent lactation intensity. Throughout the experiment, all rats were housed in standard conditions of three rats per cage, except that rats in the reproductive groups were separated to one rat per cage during the last week of pregnancy and throughout the lactation period. All groups of rats were allowed to have normal cage activities throughout the experiment. Experiments were performed in three batches, performed 5 and 28 months apart, respectively (Supplementary Table S1). Two rats in the Virgin group were euthanized after the identification of mammary tumors, two rats in the Pregnancy group and one rat in the Lactation groups failed to become pregnant, one rat each in the Lactation and Post-Weaning groups died while giving birth, and one rat in the Lactation group as well as two rats in Post-Weaning groups died during the μCT scans, resulting in a final sample size of n=8 for all groups.

2.2 In Vivo Dynamic Loading Protocol

A 2-week dynamic, compressive, uniaxial loading protocol for mouse tibia [43-45] was adapted for rats in this study. To determine the appropriate loading magnitude, a strain gauge study was performed on three separate sets of rat tibiae (methods and results described in the Supplementary Material): virgin rats at age of 4 months and 12 months, respectively, and 12-month-old reproductive rats that underwent two cycles of reproduction (n=6-8 tibiae/group).

Similar strain vs. load curves on the rat tibia midshaft were found for all three groups, indicating age and reproductive status did not significantly alter compliance of tibia to loading (Supplementary Figure S1 and Supplementary Table S4). Based on the strain gauge testing results, a pilot study of dynamic loading at a peak load of 36 N, corresponding to ~1,200 με at the tibia midshaft was conducted (n=3/group). Due to the lack of loading response at $\sim 1,200 \mu \epsilon$ detected by micro-computed tomography (µCT) analysis and dynamic histomorphometry, a peak load of 45 N, corresponding to ~1,500 με at the tibia midshaft was chosen for the current study (Figure S1 and Table S4). Briefly, rats were anesthetized (4/2% isoflurane: 4% isoflurane for induction, and 2% isoflurane for maintenance), and a peak load of 45N was applied to the left tibiae at 2 Hz (i.e., 0.15s ramp up, 0.15s ramp down, and 0.2s dwell time) by using a Bose Electroforce TestBench system (TA Instrument, Eden Prairie, MN, USA), for 5 minutes/session, 5 sessions/week over 2 weeks. The right tibia remained as a non-loaded, contralateral control. After each loading session, all rats were returned to their cages and allowed unrestricted activities. The weight of each rat was monitored during the loading period (Figure S2), and no rats were excluded from this study as the weight loss in all rats was less than 10% [45]. 2.3 In Vivo µCT Scans, Image Registration, and Bone Microstructural Analysis Micro-computed tomography (µCT) scans of both the right and left proximal tibia and tibial midshaft were performed right before (week 0) and at two weeks after the initiation of loading (week 2) using in vivo µCT (Scanco vivaCT40, Scanco Medical AG, Brüttisellen, Switzerland), as described in our previously published study [46]. Briefly, rats were anesthetized (4/2% isoflurane), and one of the tibiae was fixed into a customized holder to ensure minimal motion. A 4.2 mm thick segment of the proximal tibia (located 0.3 mm below the proximal growth plate) and a 2.1 mm thick section of the tibial midshaft (located at the midpoint between

156

157

158

159

160

161

162

163

164

165

166

167

168

169

170

171

172

173

174

175

176

177

the end of the distal and proximal epiphysis) were scanned at $10.5 \,\mu m$ voxel size. The scanner was operated at $200 \,m$ s integration time, $145 \,\mu A$ current, and $55 \,kVp$ energy, and the average scan time was approximately 30 minutes per tibia. Rats were woken up and allowed to recover for ~ 3 hours from anesthesia between the two scans performed on each tibia.

179

180

181

182

183

184

185

186

187

188

189

190

191

192

193

194

195

196

197

198

199

200

To longitudinally track the changes in trabecular microstructure within a constant volume of interest (VOI), the sequential in vivo µCT scans at the proximal tibia were aligned, using a mutual-information-based, landmark-initialized, rigid registration procedure based on open source software (National Library of Medicine Insight Segmentation and Registration Toolkit) [46, 47]. A manually contoured, 1.5-mm thick trabecular VOI, located 2.6 mm distal to the growth plate (Figure S3A&S3B), was identified in the week 2 scan and registered back to the previous scan at week 0 based on the transformation matrices that resulted from the registration, and as a result, loading-induced changes in a consistent trabecular VOI of each rat were identified and monitored (Figure 2A). Standard parameters of trabecular bone microstructure [48] were measured within each trabecular VOI. Briefly, the µCT images of trabecular bone were Gaussian filtered (sigma=1.2, support=2) and thresholded by a global threshold (corresponding to 544 mgHA/cm³), identified through an adaptive threshold function provided by the µCT scanner manufacturer. Trabecular microstructural parameters, such as bone volume fraction (BV/TV), trabecular number (Tb.N), trabecular thickness (Tb.Th), trabecular spacing, (Tb.Sp), connectivity density (Conn.D), and structure model index (SMI) were quantified. For both non-loaded and loaded tibiae of each rat, the percent change from week 0 was computed for all trabecular parameters except SMI, which ranges between -3 to 3. Normalized SMI was computed by subtracting the SMI of week 0 from week 2 measurements for each rat.

To quantify changes in cortical structure, the scans of the tibial midshaft at week 2 were registered and rotated to align with the baseline scans. A 50-slice thick cortical VOI located at the center of the tibial midshaft (Figure S3A&S3C) was semi-automatically contoured using manufacturer-provided software (Scanco Medical AG, Brüttisellen, Switzerland). Voxels within the cortical VOI were then filtered (Gaussian filter, sigma=1.2, support=2), and thresholded by application of a global threshold corresponding to 822 mgHA/cm³. Standard parameters of cortical bone microstructure, including cortical area (Ct.Area), cortical thickness (Ct.Th), and polar moment of inertia (pMOI), were measured. The percent changes in cortical bone microstructural parameters between week 0 and week 2 were calculated in both non-loaded and loaded tibiae for each rat. Moreover, the corresponding loading-induced differences in cortical microstructural percent changes between loaded vs. non-loaded tibiae (% change in loaded tibia - % change in non-loaded tibia) for each rat were further calculated.

2.4 Dynamic Bone Histomorphometry on Periosteal Bone Formation

All rats received subcutaneous injections of calcein (20 mg/kg, Sigma-Aldrich, St. Louis, MO) at day 4 of loading, and intraperitoneal injections of alizarin complexone (30mg/kg, Sigma-Aldrich, St. Louis, MO) at day 13 of loading. These injection schedules corresponded to 11 and 2 days prior to euthanasia, respectively, except in Pregnancy group (14.8±2.2 and 5.8±2.2 days prior to euthanasia, respectively). After euthanasia, ~10 mm-long segments of midshafts of both tibiae were harvested, embedded in MMA, and cut into 0.5 mm-thick transverse sections using a low-speed diamond saw (IsoMet, Buehler). ApoTome equipped Zeiss Axio Zoom.V16 microscope was applied to for image capture and subsequent digital signal correction, and the dynamic bone histomorphometry was performed to assess bone formation rate (BFR/BS), mineral apposition rate (MAR), and mineralizing surfaces (MS/BS) at the periosteal surface of

the tibial midshaft using OsteoMeasure Software (OsteoMetrics, Inc., Decatur, GA), where BS is the entire periosteal circumference [49]. The fold changes of bone formation parameters between loaded *vs.* non-loaded tibiae for each rat ((Bone formation parameters in loaded tibia - non-loaded tibia)/ non-loaded tibia) were calculated to determine the loading-induced bone formation. For samples with no double-labeled surface, the average value of MAR for the cohort to which the sample belongs was assigned for its MAR and was used to calculate BFR/BS [49]. The number of animals that had missing double-labeled surface was shown in Supplementary Table S2.

2.5 Ploton Silver Staining on Osteocyte Lacunar-Canalicular Network in the Non-loaded tibia

Immediately after euthanasia, ~15 mm-long segments of the left (non-loaded) distal tibiae starting from 2 mm proximal to the distal tibial-fibular junction were harvested, fixed in 4% paraformaldehyde (PFA) solution in phosphate-buffered saline (PBS) for 48 hours, decalcified in 10% ethylenediaminetetraacetic acid (EDTA) for 30 days, and then embedded in paraffin. 8 μm-thick longitudinal paraffin sections were prepared for the non-loaded tibiae collected from the first and second batches of 45N loading study (n=4-6/group) and the 36N loading study (n=0-2/group), making a final sample number of 6 animals per group (details shown in Supplementary Table S3).

To assess changes in lacunar-canalicular network structure, Ploton silver staining was performed on paraffin sections as previously described [40, 50]. Briefly, the de-paraffined sections were incubated in freshly mixed working silver nitrate solution, consisting of two parts of 50% silver nitrate and one part 1% formic acid in 2% gelatin (Type B gelatin from bovine skin, Sigma) solution, for 55 mins, washed in 5% sodium thiosulfate for 10 mins, and then dehydrated and mounted. Thirty lacunae were randomly selected from both medial and lateral

sides (n=15/side) on a 0.5 mm-long region of the tibial cortex located at 1 mm proximal to the distal tibial-fibular junction (n=6 rats/group) to quantify lacunar area, lacunar perimeter, the number of canaliculi emanating from each lacuna, and the number of canaliculi per lacunar surface.

2.6 Bone Immunohistochemistry (IHC) on Osteocyte PLR Activities in the Non-loaded Tibia

To assess PLR enzyme activities, paraffin sections were incubated with primary antibodies for MMP13 (1:100; Abcam, ab39012) or CtsK (1:75; Abcam, ab19027), followed by incubations with corresponding biotinylated secondary antibody, avidin-conjugated peroxidase, and diaminobenzidine substrate chromogen system (Innovex Universal Animal IHC kit) to detect positively stained cells [51]. Sections stained with Rabbit sera IgG were used as negative controls (Figure S4). All measurements were made within a 0.5-mm long region of both medial and lateral tibial diaphysis located at 1 mm proximal to the distal tibial-fibular junction. For quantification, each lacuna was manually scored as either positive or negative using OsteoMeasure Software (OsteoMetrics, Inc., Decatur, GA). Subsequently, the percentage of

2.7 Statistical Analysis

positively stained lacunae was determined.

All results are reported as mean ± standard deviation. Comparisons of loading-induced changes in the same animal, *e.g.* week 0 (pre-loading) *vs.* week 2 (post-loading), as well as left (loaded) *vs.* right (non-loaded) tibiae, were made using student's paired t-test; while one-way ANOVA with Bonferroni corrections was used to compare loading responses and osteocyte-related parameters in rats with different reproductive status. For all tests, p-values below 0.05 were considered statistically significant, while p-values below 0.1 were considered as a trend of difference with specific p-value provided.

3. Results

3.1 Effects of reproduction and lactation on trabecular and cortical bone microstructure at the
 non-loaded tibia

For the non-loaded tibiae, Virgin rats underwent minimal changes in all trabecular parameters over the 2-week period (Figure 2). In contrast, non-loaded tibiae in Pregnancy rats underwent a trend of 6% reduction in BV/TV (p=0.058), 4% and 9% reductions in Tb.N and Conn.D, respectively and a 4% increase in Tb.Sp over 2 weeks (Figure 2B-F). Moreover, for the non-loaded tibiae of Lactation rats, BV/TV, Tb.Th, Tb.N, and Conn.D dropped 20-81%, Tb.Sp increased by 87% over the 2 weeks, and SMI was 0.69 above the level at parturition (week 0, Figure 2B-G). Following weaning, the trabecular microstructure partially recovered, compared to the end of lactation. At 2 weeks post-weaning, BV/TV, Tb.Th, Tb.N, and Conn.D of non-loaded tibiae of the Post-Weaning group were elevated by 116%, 31%, 12%, and 169%, respectively, while Tb.Sp decreased by 11% and SMI lowered by 0.30 when compared to the end of lactation (week 0, Figure 2B-G). However, all trabecular bone microstructural parameters of the Post-Weaning rats (week 2) were still significantly lower than those in the age-matched virgins (Supplementary Figure S2).

In contrast to the substantial changes in trabecular bone at the proximal tibia, reproduction and lactation induced minimal alterations in cortical bone structure at the tibial midshaft (Figure 3A-C). As a result, no difference was found in any cortical bone parameters of the non-loaded tibia among groups (Figure S2). Over a 2-week period, Virgin rats underwent 0.5% and 1% increases in Ct.Area and pMOI, respectively. Moreover, Ct.Area, pMOI, and Ct.Th increased 1.5%, 2.5%, and 1.3%, respectively, over 2 weeks of pregnancy. No change was observed in Lactation rats except a trend of 1.4% decrease in Ct.Area (p=0.09) over 2 weeks of

lactation, while trends of increases of 1.2%, 0.6%, and 0.6% in Ct.Area (p=0.07), pMOI (p=0.097), and Ct.Th (p=0.07), respectively, were detected in Post-Weaning rats over the 2 weeks post-weaning.

3.2 Loading responses in trabecular bone microstructure at the proximal tibia

Two weeks of dynamic loading induced minimal loading responses in trabecular bone in Virgin, Pregnancy, and Post-Weaning groups (Figure 2). For virgin rats, no loading response was observed in trabecular bone except a 2% greater increase in Tb.Th in the loaded *vs.* non-loaded tibiae. For rats in the Pregnancy group, loading led to a greater increase in SMI in the loaded *vs.* non-loaded tibia, indicating a greater deterioration of plate-like trabeculae. Moreover, for rats in the Post-Weaning group, loading led to a trend toward reduced recovery in Conn.D. In contrast, loading reduced trabecular bone deterioration in the Lactation group (Figure 2). Although the loaded tibiae in Lactation rats still experienced a reduction in BV/TV, this bone loss was significantly attenuated by 11% when compared to the non-loaded tibiae (Figure 2B). Moreover, loading completely abolished the lactation-induced reduction in Tb.Th and attenuated the loss in Conn.D in Lactation rats (Figure 2C&2F).

3.3 Loading responses in cortical bone structure at the tibial midshaft

Significant loading responses were found in cortical bone structural parameters in all groups of rats (Figure 3A-C). The 2-week loading elevated Ct.Area, pMOI, and Ct.Th by 2.9%, 4.9%, and 2.3%, respectively, in Virgins, which were significantly greater than changes in the non-loaded tibia. Loading further enhanced the increases of Ct.Area and pMOI in the Pregnancy group to 3.8% and 6.0%. Moreover, the loading process halted the trend of lactation-induced deterioration in cortical bone structure, and further induced a 3.7% increase in pMOI. Following weaning, Ct.Area, pMOI, and Ct.Th increased by 3.6%, 6.5%, and 2.8% in the loaded tibia in

the Post-Weaning group while no change was detected in the non-loaded tibia. To further compare the extent of loading responses among groups, the differences in percent change in cortical bone structure between the loaded and non-loaded tibia were calculated for each rat (Figure 3D-F). However, no difference was found in the degree of loading responses in any cortical bone structural parameters among groups (Figure 3D-F).

3.4 Loading responses in cortical periosteal bone formation at the tibial midshaft

After two weeks of dynamic loading, MS/BS, MAR, and BFR/BS were significantly elevated in the loaded vs. non-loaded tibia in all groups (Figure 4A-D). To further compare the extent of loading responses among different groups, the fold changes in bone formation parameters between the loaded and non-loaded tibiae were derived. Intriguingly, Lactation rats had a higher fold change in MS/BS than Pregnancy and a trend towards greater fold change than Virgin rats (Figure 4E). Moreover, fold change in MAR was greater in Lactation group compared to Pregnancy and Post-Weaning groups (Figure 4F), and as a result, Lactation rats had the highest loading-induced fold change in BFR/BS among all groups (Figure 4G).

3.5 Effects of reproduction and lactation on osteocyte lacunar-canalicular network structure and PLR activities

Qualitatively, no distinct differences in the lacunar-canalicular network were observed among groups (Figure 5A). Quantitative comparisons indicated that the lacunar perimeter was 10%, 7%, and 8% greater in Lactation rats when compared to Virgin, Pregnancy, and Post-Weaning groups, respectively (Figure 5B). Similarly, Lactation rats had 15-21% greater lacunar area than all other groups (Figure 4C). No difference was detected in the number of canaliculi emanating from one lacuna or in the number of canaliculi per lacunar surface (Figure 5D&5E).

Significant PLR enzymatic activities were detected in Lactation rats. The percentage of MMP13-positive osteocytes was 37% and 40% greater in Lactation than Virgin and Post-Weaning rats, respectively (Figure 6A&6B). Similarly, percentage of osteocytes that stained positive for CtsK was 50% higher in Lactation than Post-Weaning rats (Figure 6C&6D).

4. Discussion

This study was the first investigation on the effects of dynamic loading on bone health during pregnancy, lactation, and post-weaning recovery in an *in vivo* animal model. By applying a dynamic tibial loading protocol with 1,500 µE at tibial midshaft to mimic jogging or running in women, we demonstrated that despite the minimal loading responses detected at the trabecular bone in virgins, loading reduced lactation-induced trabecular bone loss and improved cortical bone structure regardless of reproductive status, indicating a beneficial effect of weight-bearing exercise on maternal bone during pregnancy and postpartum. Moreover, loading led to greater periosteal bone formation in lactating rats compared to rats at other reproductive stages or agematched virgins, indicating a greater mechano-responsiveness of maternal bone during lactation.

Variable results were reported in clinical investigations regarding the effect of weight-bearing activities during pregnancy and post-partum [27-30]. Discrepancies may be due in part to inconsistencies in voluntary exercise intensity and differences in the stage of reproduction and lactation among studies. By applying dynamic loading to rats at well-defined reproductive stages, the current study directly evaluated the potential of load-bearing exercise to modulate bone responses to reproduction and lactation. We applied a 2-week dynamic tibial compressive loading that induced a peak of ~1,500 με near the lateral mid-shaft surface, which mimics jogging or running in women [52, 53]. Minimal loading responses were observed in trabecular bone at the proximal tibia in virgin, pregnancy and post-weaning rats, while a significant loading

response was detected in trabecular bone of lactation rats, indicating a loading-induced attenuation in trabecular bone loss during lactation. However, despite attenuated trabecular bone loss during lactation, the absolute values of trabecular microstructural parameters in Lactation rats were still lower than the age-matched virgins. In contrast, dynamic loading enhanced cortical bone structure and periosteal bone formation in all groups, suggesting that weight-bearing exercise at moderate intensity exerts a protective effect or enhancement on cortical bone in rats regardless of their reproductive stage. Furthermore, intriguingly, the loading-induced increase in bone formation rate at the periosteal cortex of the tibial midshaft in lactating rats was greater than that observed in virgins or other reproductive groups, indicating a greater mechanoresponsiveness of cortical bone during the lactation period. Consistent with our findings, a previous study conducted ex vivo loading on the mouse fibula, and found a stronger loadinginduced reduction in osteocytic sclerostin expression as well as a greater elevation in β-catenin expression by osteocytes in lactating mice than age-matched virgins, suggesting that the osteocytes in fibulae from lactation mice may have a stronger response to mechanical loading [54]. The enhanced loading responses in both trabecular and cortical bone during the lactation period further emphasize the beneficial effects of physical exercises on maternal bone health postpartum.

361

362

363

364

365

366

367

368

369

370

371

372

373

374

375

376

377

378

379

380

381

382

383

Our longitudinal µCT imaging approach allowed for the tracking of local changes in the trabecular and cortical bone within a constant volume of interest (VOI) over the 2-week period during pregnancy, lactation, and post-weaning recovery in both loaded and non-loaded tibiae. As expected, reproduction and lactation induced substantial alterations in trabecular bone microstructure at the proximal tibia, which aligns with several previously published studies [14, 22, 23]. For the first time, structural changes at the tibial midshaft cortex were monitored by

using in vivo µCT imaging. During pregnancy, a small but significant increase in cortical bone size at the tibia midshaft was detected. This is similar to what has been reported in the tibial metaphysis, where the tibial cortex significantly increased, compensating the trabecular bone deterioration during pregnancy [22]. Our results also indicated a trend of reduction in cortical bone parameters at the tibial midshaft during lactation. In agreement with our findings, several rodent studies suggested that the adverse effects of lactation are less pronounced at the predominantly cortical tibial and femoral midshaft [16, 21, 55, 56]. These µCT-based findings were further confirmed by the results of our dynamic histomorphometry analysis, which align well with previous findings that the periosteal bone formation was elevated during pregnancy, and ceased during lactation [17]. Following weaning, only trends of tiny increases in tibial midshaft cortex was detected in the current study. This is consistent with previous investigations in femoral midshaft of rats and mice, which suggested that the cortical bone structure still remains deteriorated post-weaning when compared to virgins [16, 21, 25, 57, 58]. Nevertheless, previous studies suggested that improvements in intrinsic tissue mechanical properties may compensate the cortical bone structural deficit, resulting in no difference in femoral stiffness or peak load between post-weaning and virgin bone [24, 25]. Taken together, at the critical loadbearing sites such as the tibia or femur midshaft, the significant improvement in cortical bone structure during pregnancy, less pronounced reduction at cortical bone during lactation, and further improvements in material properties after weaning may work together to offset the potential loss of strength induced by trabecular bone deficit following reproduction and lactation. Consistent with previous studies in CD1 and C57BL/6 mice [35, 36, 39, 40, 59], our study further confirmed that lactation resulted in increased lacunar size and osteocytic PLR

enzyme activities in rats, and these transient changes were reverted post-weaning. No significant

384

385

386

387

388

389

390

391

392

393

394

395

396

397

398

399

400

401

402

403

404

405

changes in lacunar morphology were observed during pregnancy. Moreover, no striking changes in canalicular network were observed throughout the whole reproductive cycle, which agrees with previous findings in mice [39]. In contrast to our findings, a previous study evaluating lacunar diameter using μ CT with a voxel size of 2 μ m found no difference between lactation and virgin rats on normal diet [58]. Give the small size of lacunae (~10 μ m in the short axis [34]) and the subtle change during lactation (7~10% increase in perimeter), the limited image resolution of μ CT may not allow the detection of such small changes in LCS induced by lactation. Another study using Naval Medical Research Institute (NMRI) mice also reported no lactation-associated changes in lacunar size and morphology, suggesting that the effects of lactation on lacunar structure may be strain-dependent in rodents [60].

The total surface area of osteocyte lacunae has been estimated to be several magnitudes larger than that of the trabecular bone surfaces upon which osteoclasts can act, and as a result, small alterations in osteocyte lacunae and canaliculi through PLR during lactation may lead to a substantial change in bone mineral content at the level of the whole animal [39, 61].

Additionally, the LCS structure, particularly the pericellular matrix (PCM) in the LCS, also plays a critical role in osteocyte mechano-transduction. It has been suggested that the interstitial fluid flow in the LCS, driven by external mechanical loading, may amplify tissue-level strains for osteocytes to sense and respond to [34, 62, 63]. Through PLR, the lactation-associated changes in LCS and its PCM may have an impact on the mechanical signals perceived by osteocytes and their cell processes, leading to altered bone mechano-responsiveness. To understand the potential impact of PLR on osteocyte mechanosensing, Lai *et al.* [42] quantified and compared the loading-induced fluid flow, flow-mediated mechanical stimulation on osteocytes, and solute transport in LCS in the lactating and nulliparous skeleton using a multiscale modeling approach

built upon the LCS fluid flow model established by Weinbaum et al. [64] and experimental and modeling system developed by Wang et al. [43, 63, 65]. Using the key LCS features based on published experimental data of lactating and nulliparous murine tibiae, the model predicted that increased LCS porosity alone would lead to a marked increase of fluid drag force on the osteocyte body and cell processes under a high frequency (4Hz) loading. Furthermore, the increased LCS dimensions will lead to increased transport flux of signaling molecules, nutrients, and waste products among osteocytes and between osteocytes and cells residing on the bone surface. Moreover, degradation of the PCM fibers, which most possibly would occur in matrix lysis [35, 37, 66], along with high frequency loading, would synergistically promote flowmediated mechanical stimulations on osteocytes and their cell processes, and enhance solute transport in the LCS. Based on these modeling results, we hypothesized that lactation-induced structural changes of the LCS and its PCM alter the microenvironment of osteocytes, leading to enhanced osteocyte mechanosensing. Aligning with our working hypothesis, osteocyte lacunae in aging mice are smaller and more spherical, with reduced PCM density [43, 67], which has been suggested to be associated with the reduced bone mechano-responsiveness with aging [68, 69]. Further studies are warranted to explore the effects of reproduction and lactation on osteocyte LCS ultrastructure, pericellular space and fiber density, and to experimentally establish their direct influences on the load-induced, fluid-mediated mechanical signals on osteocytes and other bone cells. In addition to the positive effects of dynamic loading during pregnancy and post-partum on maternal bone, the mother's participation in physical activities may affect the offspring.

Although we did not investigate the effects of dynamic loading during pregnancy and lactation

on fetal/infant development in our current study, no obvious difference in the size of neonatal

430

431

432

433

434

435

436

437

438

439

440

441

442

443

444

445

446

447

448

449

450

451

pups or subsequent growth rate of pups was observed throughout the experiment when compared to the "normal litters" from mothers with standard cage activities. Intriguing, a recent study recruited 141 women and categorized them into different activity groups based on activity types and intensities, and found no relationship between physical activity during pregnancy and neonatal birth weight [70]. Another recent study showed that increased levels of physical activity by pregnant women are associated with improved breastfeeding outcomes, which may benefit their offspring [71]. Moreover, it has been suggested that moderate exercise does not affect milk supply, milk macronutrient and mineral composition, or infant growth [72]. Taken together, a moderate level of dynamic loading during pregnancy and postpartum appears to exert no adverse effects on the offspring.

Our study was not without limitations. Firstly, the effects of reproduction and lactation on osteocyte LCS network and PLR activities were not examined in the loaded tibiae. Our study was designed with the primary objective of investigating the loading responses in rats with different reproductive status, while the secondary objective was to examine the alterations of lacunar-canalicular system (LCS) over the reproductive cycle. Therefore, the proximal tibiae and tibial midshafts were embedded in MMA to assess loading responses, while only the distal tibiae were harvested for paraffin embedding to assess LCS network and PLR activities. Previous studies have suggested that the strain level experienced at rat distal tibia is much lower compared with the tibial midshaft, indicating that the distal tibia is not an ideal location to analyze loading effects [73]. Moreover, a recent study found that the loading process with 700-1,200 µε peak led to 20% increase in canalicular length and elevated PLR mRNA level at the proximal tibia, but no loading-induced difference was detected in the distal tibia, indicating that the mechanoregulation of PLR was site-specific [74]. Therefore, future studies that are designed to directly assess PLR

at the proximal tibia, are warranted to investigate the loading-induced effects on LCS network and PLR activities. Secondly, the ideal strain gauge measurements to identify loading magnitude should be conducted in rats with the same age of 7 months, however, the current strain gauging study was performed in rats with different ages and reproductive status, including 4-month-old virgin female rats, 12-month-old virgin female rats, and 12-month-old reproductive rats (n=6-8 tibiae/group). Similar strain-load curves were observed in all groups of female rats, indicating that age and reproductive status did not significantly alter compliance of tibia to loading, and thus, we expect that the tibia of rats at age of 7 months would share a similar strain-load relationship with those of other female groups. Moreover, the maternal trabecular bone underwent rapid changes during pregnancy, lactation, and post-weaning recovery, making it difficult to adjust the peak load to achieve consistent tissue strains over the 2-week loading period. Therefore, a 45N peak load, corresponding to ~1,500 με on the tibial midshaft surface in virgin rats, was applied to all reproductive groups. However, reduced trabecular bone volume and deteriorated microstructure in the Lactation and Post-Weaning rats may lead to different strain distributions inside the trabecular bone compartment when compared to Virgin and Pregnancy groups. Nevertheless, the majority of the load applied to long bone is carried by the cortical bone compartment. In the current study, no difference was found in the tibial midshaft structure among groups (Figure S2). Therefore, we expect the average tissue strains applied to the tibial midshaft to be comparable among groups. To further derive and compare the mechanosensitivity of maternal bone at different reproductive stages, additional pilot experiments with peak load at ~1,200 and ~1,800 με surface strain were conducted (data not shown). However, while minimal loading responses were observed at \sim 1,200 µE (36N), the loading experiment at ~1,800 µE was terminated early due to the soft tissue damage in the rat joint caused by the high

476

477

478

479

480

481

482

483

484

485

486

487

488

489

490

491

492

493

494

495

496

497

peak load (54N). To overcome this limitation, a mouse model will be established in our future studies, where a greater range of strains of 1,200-2,000 με on the medial bone surface can be safely applied to induce robust adaptive loading responses on the tibia [45].

Despite these shortcomings, our study provided a thorough evaluation of the effects of pregnancy, lactation, and weaning on maternal bone mechano-responsiveness and osteocyte microenvironment in rats. By applying a dynamic loading protocol, we demonstrated the beneficial effect of loading on enhancing cortical bone structure of maternal bone during pregnancy, lactation, and post-weaning recovery. Particularly, maternal bone during lactation exhibited a greater mechano-responsiveness to dynamic loading in both trabecular and cortical bone compartments when compared to Virgin, Pregnancy, and Post-Weaning rats. Furthermore, elevated osteocyte PLR activities during lactation resulted in significantly increased osteocyte lacunar dimensions in lactating rats. This may lead to changes in interstitial fluid flow-mediated mechanical stimulation on osteocytes and increased solute transport in the LCS during high-frequency dynamic loading, thus enhancing mechano-responsiveness of maternal bone during lactation. Taken together, this study provides important insight into the relationship between reproduction and lactation-induced skeletal changes and external mechanical loading, emphasizing the importance of weight-bearing exercise on maternal bone health postpartum.

5. Acknowledgements

We thank Dr. Tamara Alliston and Dr. Cristal Yee, University of California, San Francisco, for kindly providing the protocols of Ploton silver staining and immunohistochemistry of MMP13 and CtsK.

Research reported in this publication was supported by the Penn Center for Musculoskeletal Diseases (PCMD) NIH/NIAMS P30-AR069619, NIH/NIAMS R01-AR071718

- 522 (to XSL), NIH/NIAMS F32-AR076906 (to RC), and National Science Foundation (NSF) Award
- 523 #1653216 (to XSL).

524 Figures:

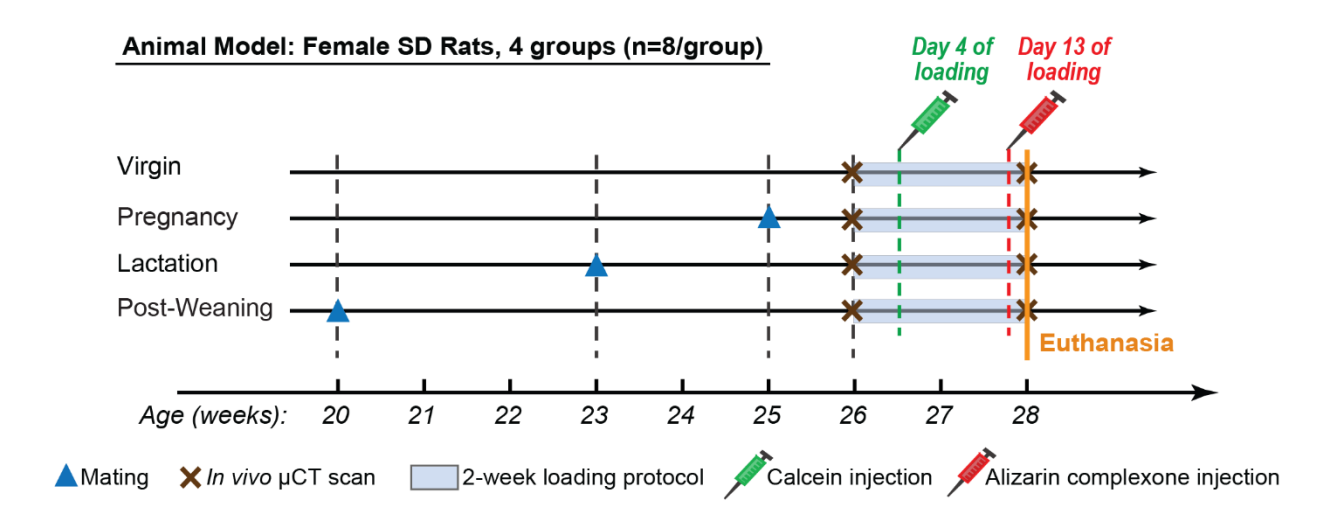


Figure 1. Schematics of study design.

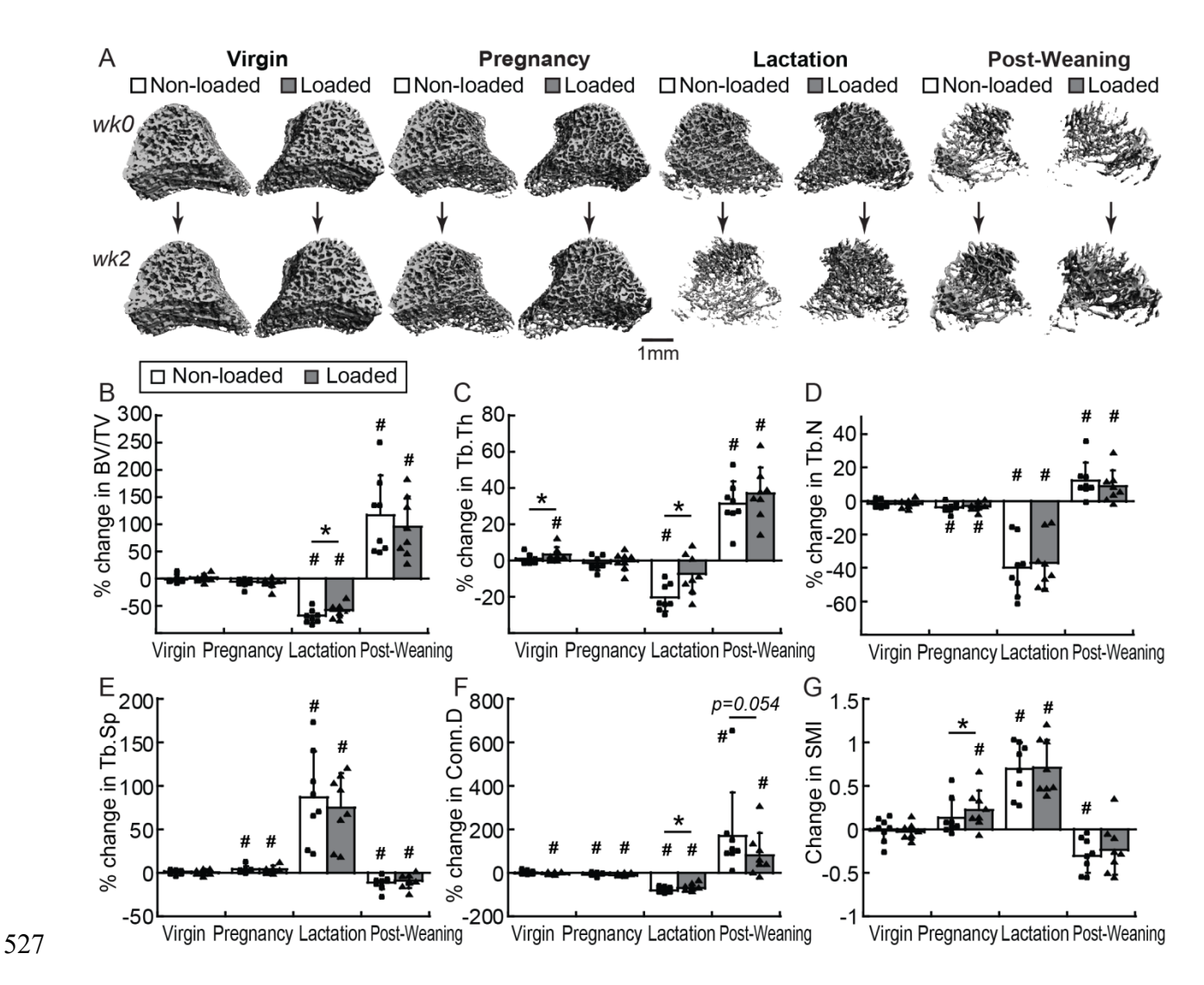


Figure 2. (A) Representative 3D renderings of trabecular bone at the proximal tibia in Virgin, Pregnancy, Lactation, and Post-Weaning rats. % changes in (B) BV/TV, (C) Tb.Th, (D) Tb.N, (E) Tb.Sp, and (F) Conn.D, as well as (G) change in SMI in loaded and non-loaded tibiae in rats with different reproductive status. p<0.05: # indicates significant changes over the 2-week time period (week 0 *vs.* week 2); * indicates significant differences between loaded and non-loaded tibiae.

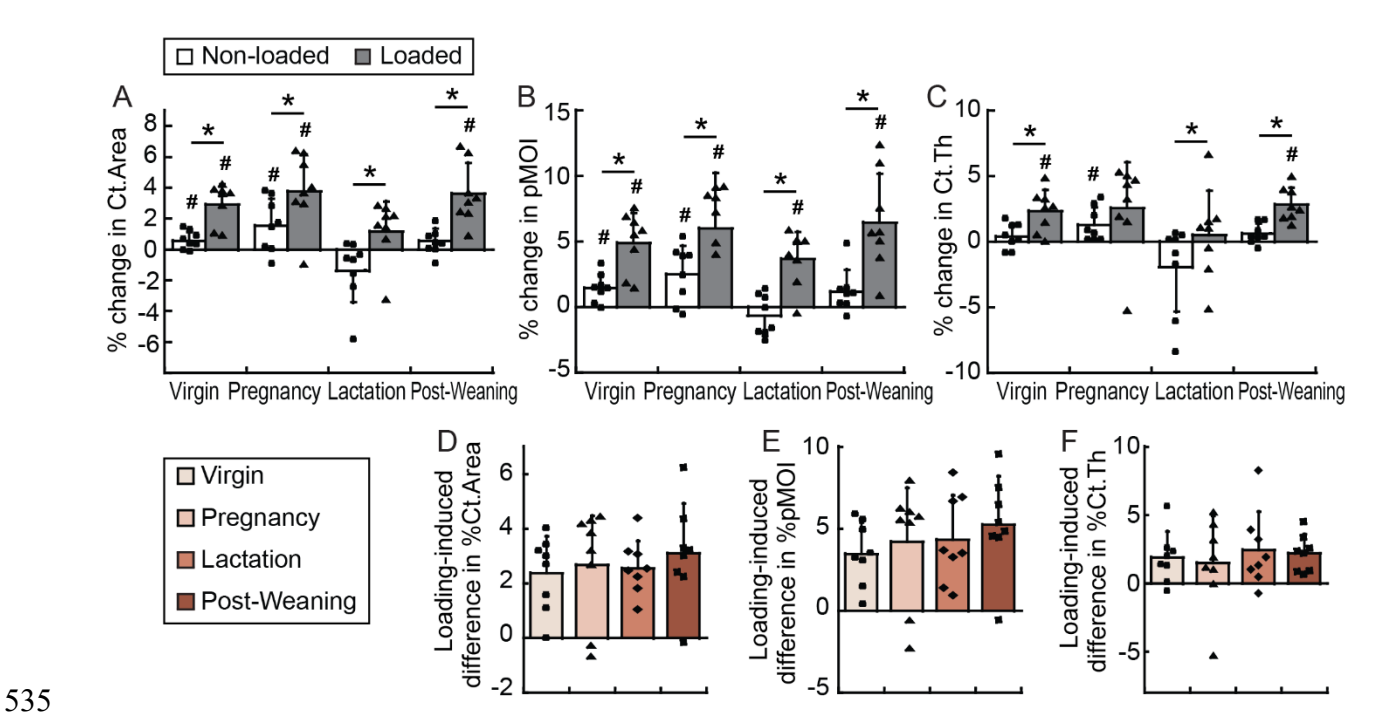


Figure 3. % changes in (A) Ct.Area, (B) pMOI, and (C) Ct.Th at tibial midshaft in loaded and non-loaded tibiae in rats with different reproductive status. Comparisons of loading-induced differences in % change between loaded and non-loaded tibiae in (D) Ct.Area, (E) pMOI, and (F) Ct.Th at tibial midshaft in rats with different reproductive status. p<0.05: # indicates significant changes over the 2-week time period (week 0 *vs.* week 2); * indicates significant differences between loaded and non-loaded tibiae.

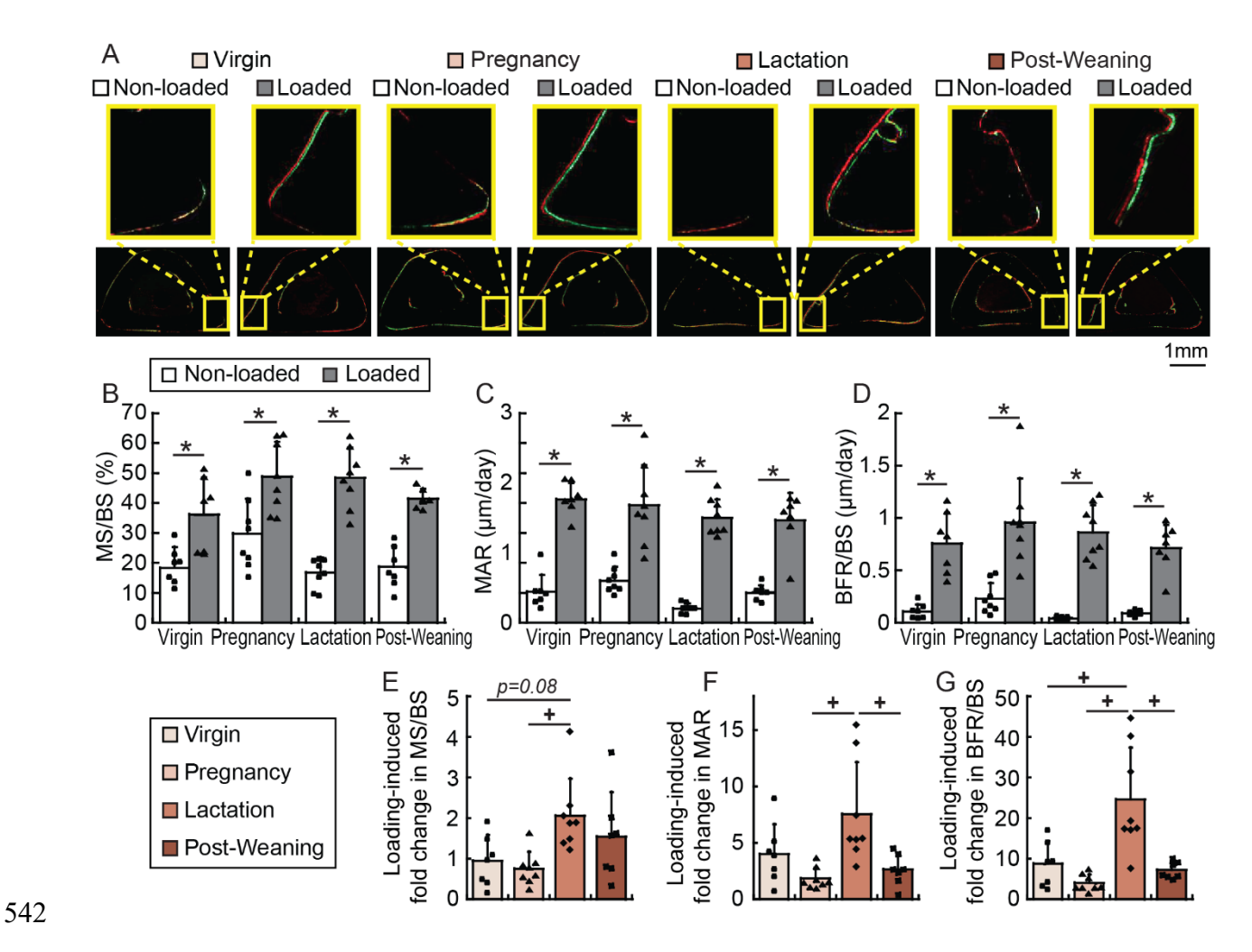


Figure 4. (A) Representative histology images of tibial midshaft. Comparisons of (B) MS/BS, (C) MAR, and (D) BFR/BS at periosteal cortical bone of tibial midshaft between loaded and non-loaded tibiae in rats with different reproductive status. Comparisons of loading-induced fold changes in periosteal (E) MS/BS, (F) MAR, and (G) BFR/BS at tibial midshaft in rats with different reproductive status. p<0.05: * indicates significant differences between loaded and non-loaded tibiae; + indicates significant differences in loading-induced fold change among groups.

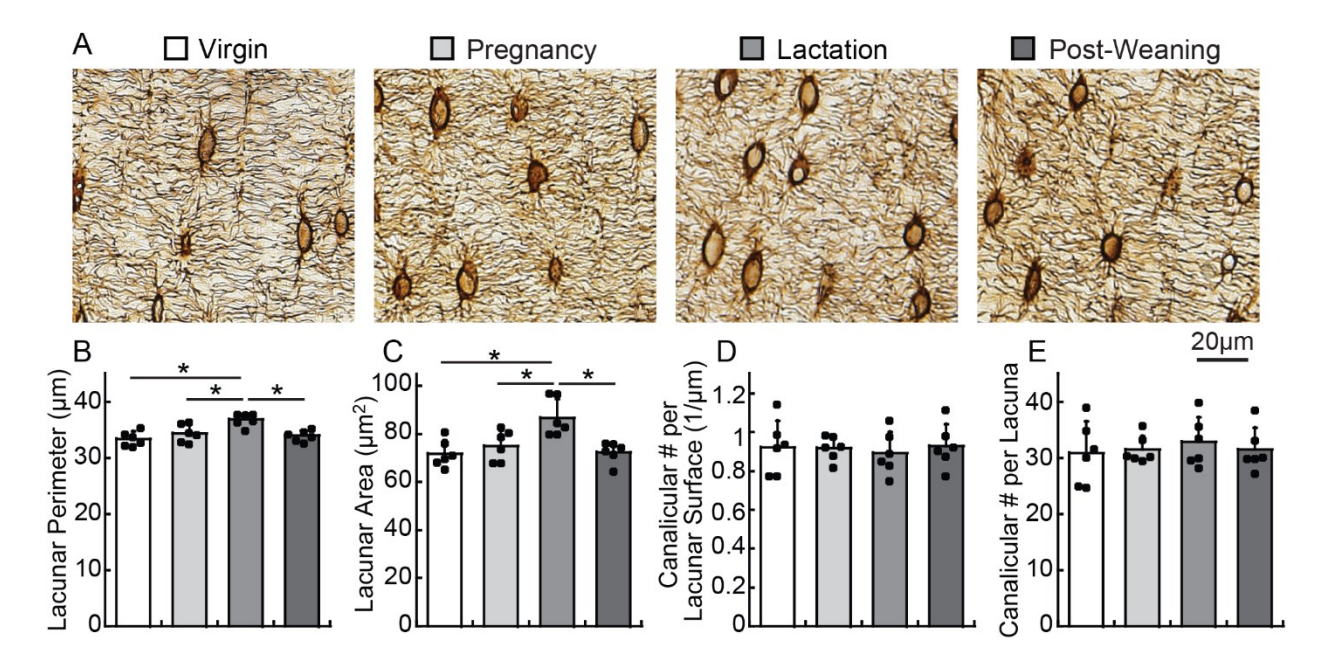


Figure 5. (A) Representative images of lacunar-canalicular network by Ploton silver staining. Comparisons of (B) lacunar perimeter, (C) lacunar area, (D) canalicular number per lacunar surface, and (E) canalicular number per lacuna at tibial cortex in rats with different reproductive status. * indicates significant differences among groups (p<0.05).

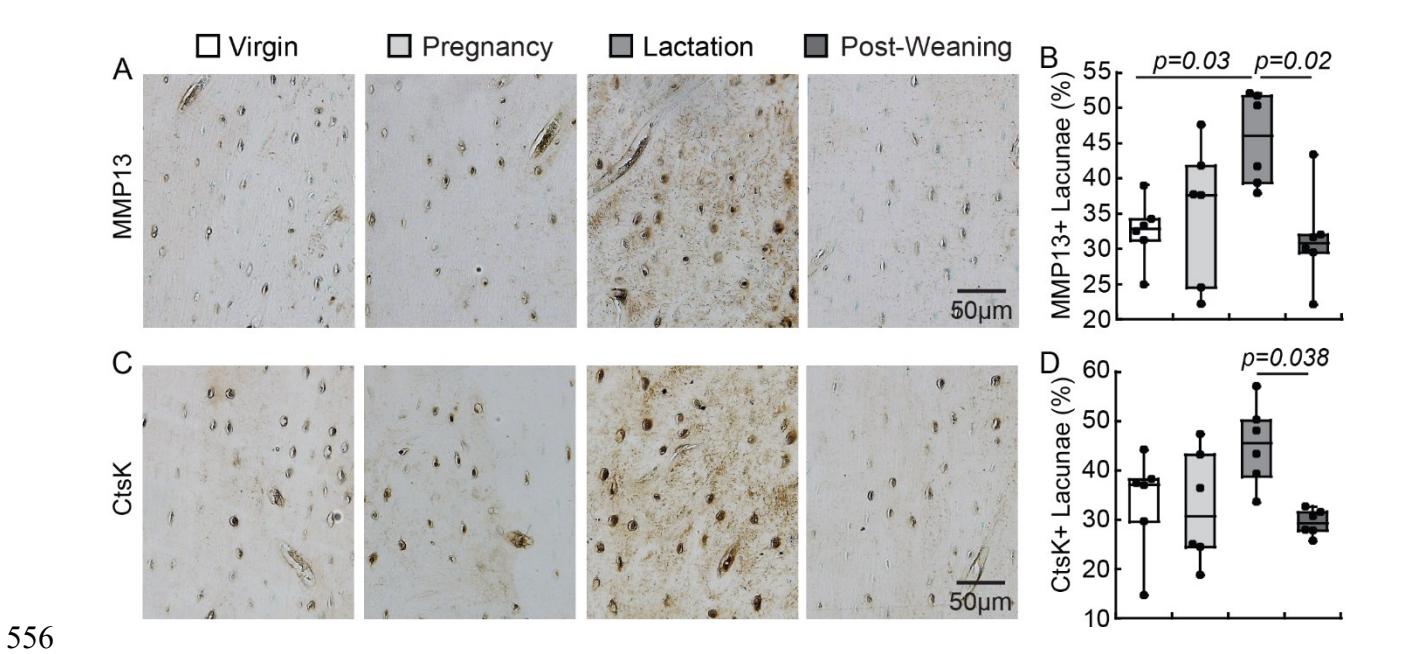


Figure 6. Representative images of (A) MMP13 and (C) CtsK immunostaining. Comparisons of (B) % MMP13-postive and (D) CtsK-postive osteocytes at tibial cortex in rats with different reproductive status. * indicates significant differences among groups (p<0.05).

Supplementary Materials

560

561

562

563

564

565

566

567

568

569

570

571

572

573

574

575

576

577

578

579

580

581

582

Methods of strain gauge study:

A separate set of rats, including 4-month-old male rats, 4-month-old virgin female rats, 12month-old virgin female rats, and 12-month-old reproductive rats, were utilized for ex vivo strain gauging experiment to determine the required load magnitude (n=6-8 tibiae/group) of the dynamic compressive loading protocol. Reproductive rats underwent 2 cycles of pregnancy, with each cycle consisting of a 3-week lactation and a 6-week post-weaning recovery period, followed by euthanasia 8 weeks after the end of the 2nd cycle. A single-element gauge (EA-06-015DJ-120; Measurements Group, Inc., Raleigh, NC) was attached on the relatively flat medial surface (1-2 mm proximal of tibial mid-diaphysis) of the intact tibia that remained attached to the rat body. A compressive loading with gradually increased magnitude (0.5N/s to 60N) was applied to the tibia by utilizing a Bose Electroforce TestBench® loading system (TA Instrument, Eden Prairie, MN, USA), and the corresponding output voltage of the strain gauge was automatically recorded by LM1's data acquisition unit and converted to strain by applying a calibrated conversion coefficient. The compressive rigidity of tibiae for each group of rats was calculated from the strain-load curves derived from the loading tests. To achieve a consistent 1500 µs strain on the tibial surface, the loading magnitudes for the four groups of rats were calculated to be 55.8±3.4 N, 44.0±3.2 N, 44.9±4.2N, and 44.7±7.0N for 4-month-old males, 4-month-old virgin females, 12-month-old virgin females, and 12-month-old reproductive females, respectively (Table S4). Based on the similar strain-load curves observed in all groups of female rats regardless of age or reproductive status (Fig S1), we expect that the tibia of rats at age of 7 months would share a similar strain-load relationship with those of other female groups. In our pilot study, a peak load of 36N (corresponding to ~1200 με on the surface of tibial midshaft) was

applied to the 7-month-old female rats, but minimal loading responses were detected (data not shown). Therefore, a loading magnitude of 45N, which corresponds to a higher strain of \sim 1500 $\mu\epsilon$ on the tibial midshaft surface, was utilized to induce adaptive loading responses in the current study in all groups of rats.

Table S1: Number of rats per group from each batch

Consess	Animal number in each batch (n)				
Group	Batch 1	Batch 2	Batch 3		
Virgin	3	5	2		
Pregnancy	3	3	4		
Lactation	3	4	4		
Post-Weaning	3	4	4		

Table S2: Number of rats with missing double-labeled surface in each group

Group	Number of rats with missing double-labeled surface		
Virgin	2		
Pregnancy	1		
Lactation	4		
Post-Weaning	2		

Sample number of non-loaded tibia in each study (n) Group Pilot study (36N) Main study (45N) 0 Virgin 6 Pregnancy 2 4 Lactation 5 1 Post-Weaning 1 5

Strains	Magnitude of Compressive Load Required (N) *					
(με)	4mo Male	4mo Virgin Female	12mo Virgin Female	12mo Reproductive Female		
500	18.6 ± 1.1	14.7 ± 1.1	15.0 ± 1.4	15.0 ± 2.3		
750	27.9 ± 1.6	22.0 ± 1.6	22.5 ± 2.1	22.4 ± 3.5		
1000	37.2 ± 2.2	29.3 ± 2.1	29.9 ± 2.8	29.8 ± 4.7		
1250	46.5 ± 2.8	36.6 ± 2.7	37.4 ± 3.5	37.3 ± 5.9		
1500	55.8 ± 3.4	44.0 ± 3.2	44.9 ± 4.2	44.7 ± 7.0		
1800	67.0 ± 4.1	52.7 ± 3.8	53.9 ± 5.0	53.7 ± 8.4		

^{*:} Data represented as mean \pm SD.

Table S5: Trabecular and cortical bone microstructural parameters at week 2 in non-loaded and loaded tibiae in rats with different reproductive status

Structural	Virgin		Pregnancy		Lactation		Post-Weaning	
Parameters (at week 2)	Non-loaded	Loaded	Non-loaded	Loaded	Non-loaded	Loaded	Non-loaded	Loaded
Proximal tibia								
BV/TV	0.28 ± 0.09	0.29 ± 0.08	0.26 ± 0.05	0.27 ± 0.04	0.05 ± 0.03	$0.07\pm0.03*$	0.08 ± 0.05	$0.10\pm0.06 \textcolor{red}{\ast}$
Tb.Th (mm)	0.071 ± 0.008	0.072 ± 0.008 *	0.067 ± 0.004	0.067 ± 0.003	0.047 ± 0.004	$0.054 \pm 0.006 *$	0.060 ± 0.010	$0.067 \pm 0.008 *$
Tb.N (1/mm)	5.39 ± 1.07	5.16 ± 0.92	5.37 ± 0.84	5.26 ± 0.86	2.80 ± 0.82	2.89 ± 1.04	2.80 ± 0.82	2.87 ± 0.77
Tb.Sp (mm)	0.17 ± 0.03	0.18 ± 0.03	0.17 ± 0.03	0.17 ± 0.03	0.43 ± 0.21	0.39 ± 0.15	0.39 ± 0.16	0.38 ± 0.15
Conn.D (1/mm ³)	166.8 ± 64.2	158.8 ± 52.3	166.8 ± 64.2	168.8 ± 64.5	22.1 ± 23.1	33.9 ± 29.6	28.1 ± 21.8	34.8 ± 23.5
SMI	1.54 ± 0.32	$1.14\pm0.61*$	1.54 ± 0.32	1.45 ± 0.21	2.99 ± 0.26	2.90 ± 0.23	2.76 ± 0.49	2.87 ± 0.57
Tibial midshaft								
pMOI (mm ⁴)	5.23 ± 0.86	$5.60 \pm 1.07 *$	5.50 ± 0.80	$6.00\pm0.86 \textcolor{white}{\ast}$	5.22 ± 0.64	$5.79 \pm 0.73*$	5.52 ± 1.16	$6.23 \pm 1.26*$
Ct.Area (mm²)	4.18 ± 0.35	$4.37\pm0.36 *$	4.29 ± 0.25	$4.46 \pm 0.23*$	4.18 ± 0.18	$4.39\pm0.22*$	4.22 ± 0.43	$4.47\pm0.41 \textcolor{red}{\ast}$
Ct.Th (mm)	0.58 ± 0.03	$0.60\pm0.02 \textcolor{red}{\ast}$	0.59 ± 0.03	0.6 ± 0.02	0.58 ± 0.03	$0.59\pm0.02\boldsymbol{*}$	0.57 ± 0.03	$0.59 \pm 0.03 *$

Data represented as mean \pm SD.

594

^{*:} Loaded different from non-loaded tibia, p<0.05.

Figure S1: Relationships between strains ($\mu\epsilon$) on the surface of the tibial midshaft and the corresponding magnitude of compressive load required (N) in 4-month-old male rats, 4-month-old virgin female rats, 12-month-old virgin female rats, and 12-month-old reproductive female rats.

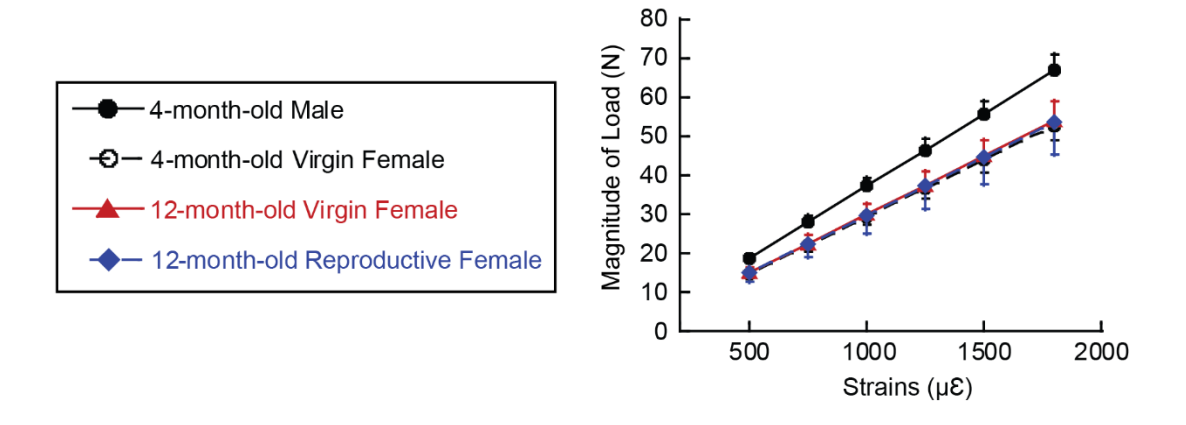


Figure S2: Weight of rats before (week 0) and after loading (week 2). * indicates significant 602 difference over the loading period (p<0.05).

601

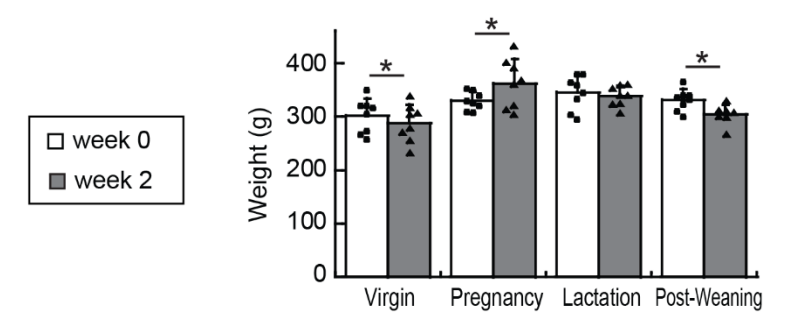


Figure S3: (A) Illustrations of μCT scanning regions and VOIs for analysis. Region between green dash lines is the scanning region at proximal tibia; green rectangle represents the VOI for trabecular bone analysis. Region between orange dash lines is the scanning region at tibial midshaft; orange rectangle represents the VOI for cortical bone analysis. (B) Representative 3D renderings of trabecular bone at the proximal tibia. (C) Representative 3D renderings of cortical bone at the tibial midshaft.

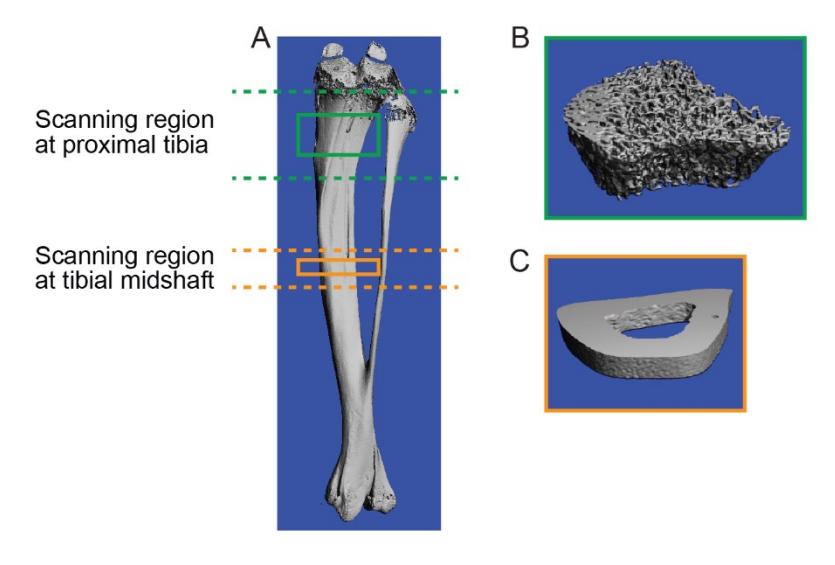


Figure S4: Representative images of negative controls of MMP13 and CtsK IHCs

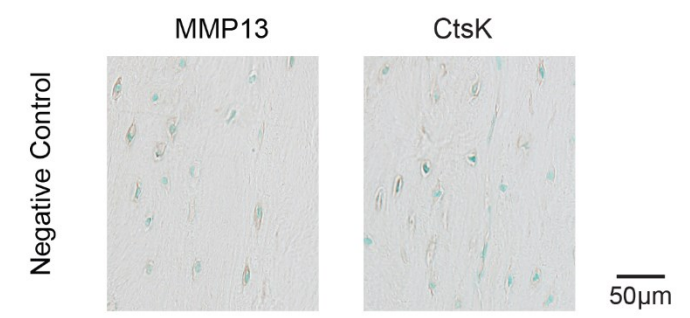
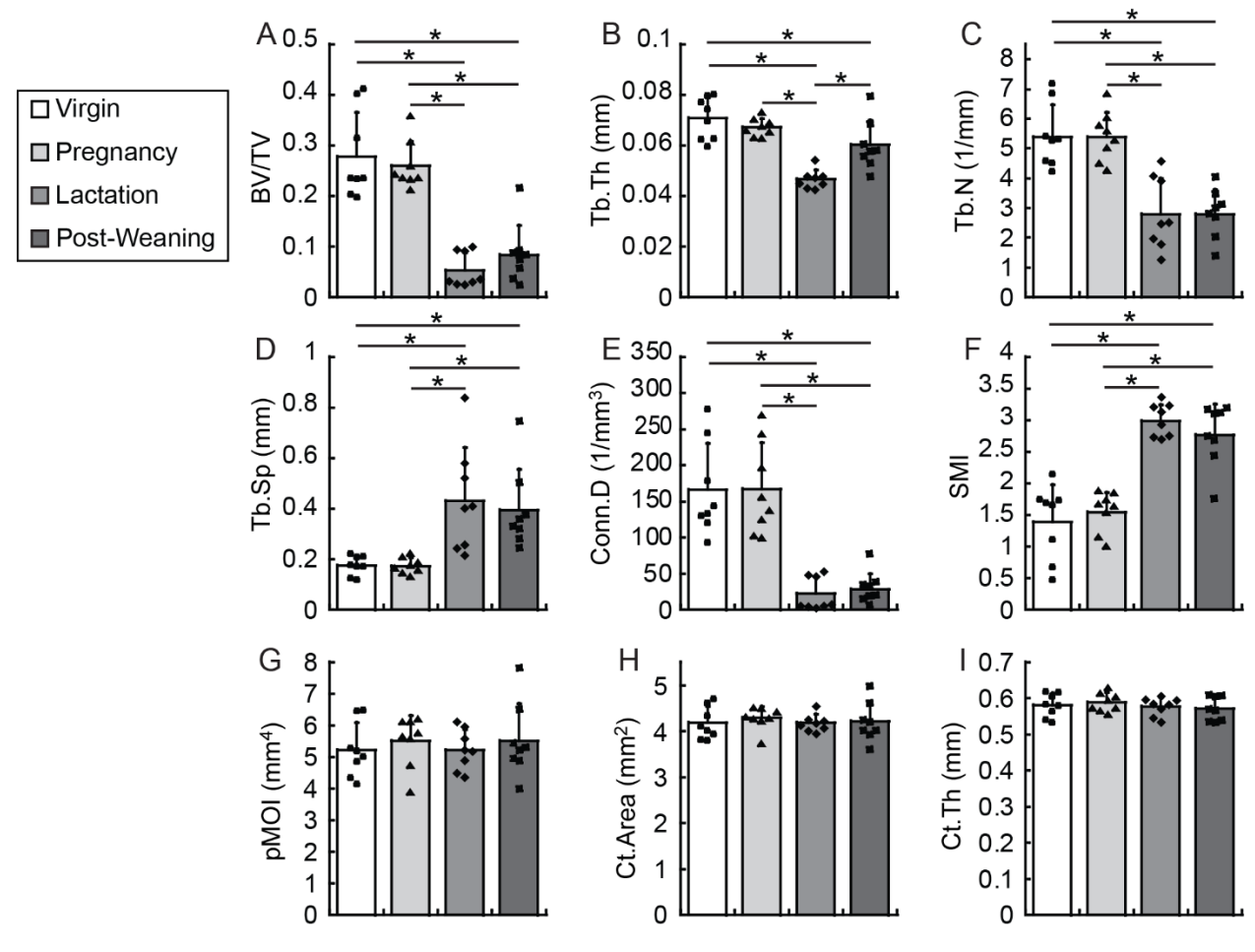


Figure S5: Trabecular microstructural parameters at proximal tibia in rats at different reproductive stages, including: (A) BV/TV, (B) Tb.Th, (C) Tb.N, (D) Tb.Sp, (E) Conn.D, and (F) SMI. Cortical bone structural parameters at tibial midshaft in rats at different reproductive stages, including: (G) pMOI, (H) Ct.Area, and (I) Ct.Th. * indicates significant difference among groups (p<0.05).



References:

- Kovacs, C.S., Maternal Mineral and Bone Metabolism During Pregnancy, Lactation, and
 Post-Weaning Recovery. Physiol Rev, 2016. 96(2): p. 449-547.
- 622 2. Black, A.J., et al., A detailed assessment of alterations in bone turnover, calcium
- *homeostasis, and bone density in normal pregnancy.* J Bone Miner Res, 2000. **15**(3): p. 557-63.
- Moller, U.K., et al., Changes in bone mineral density and body composition during pregnancy and postpartum. A controlled cohort study. Osteoporos Int, 2012. **23**(4): p. 1213-23.
- Kaur, M., et al., Longitudinal changes in bone mineral density during normal pregnancy.
 Bone, 2003. **32**(4): p. 449-54.
- Naylor, K.E., et al., *The effect of pregnancy on bone density and bone turnover.* J Bone Miner Res, 2000. **15**(1): p. 129-37.
- 632 6. Pearson, D., et al., *Recovery of pregnancy mediated bone loss during lactation*. Bone, 2004. **34**(3): p. 570-8.
- 634 7. Sowers, M., et al., *Changes in bone density with lactation*. JAMA, 1993. **269**(24): p. 3130-5.
- 636 8. Karlsson, C., K.J. Obrant, and M. Karlsson, *Pregnancy and lactation confer reversible bone loss in humans*. Osteoporos Int, 2001. **12**(10): p. 828-34.
- 638 9. Kent, G.N., et al., *Human lactation: forearm trabecular bone loss, increased bone*639 turnover, and renal conservation of calcium and inorganic phosphate with recovery of
 640 bone mass following weaning. J Bone Miner Res, 1990. **5**(4): p. 361-9.
- Honda, A., et al., *Lumbar bone mineral density changes during pregnancy and lactation.*Int J Gynaecol Obstet, 1998. **63**(3): p. 253-8.
- Kalkwarf, H.J., et al., *The effect of calcium supplementation on bone density during lactation and after weaning.* N Engl J Med, 1997. **337**(8): p. 523-8.
- Wysolmerski, J.J., *Interactions between breast, bone, and brain regulate mineral and skeletal metabolism during lactation.* Ann N Y Acad Sci, 2010. **1192**: p. 161-9.
- Liu, X.S., et al., *Mechanical Regulation of the Maternal Skeleton during Reproduction* and Lactation. Curr Osteoporos Rep, 2019. **17**(6): p. 375-386.
- 649 14. Bowman, B.M., C.C. Siska, and S.C. Miller, *Greatly increased cancellous bone*650 formation with rapid improvements in bone structure in the rat maternal skeleton after
 651 lactation. J Bone Miner Res, 2002. **17**(11): p. 1954-60.
- 652 15. Miller, S.C., B.L. Anderson, and B.M. Bowman, *Weaning initiates a rapid and powerful anabolic phase in the rat maternal skeleton*. Biol Reprod, 2005. **73**(1): p. 156-62.
- 654 16. Ardeshirpour, L., et al., Weaning triggers a decrease in receptor activator of nuclear 655 factor-kappaB ligand expression, widespread osteoclast apoptosis, and rapid recovery of 656 bone mass after lactation in mice. Endocrinology, 2007. **148**(8): p. 3875-86.
- 657 17. Miller, S.C. and B.M. Bowman, *Rapid improvements in cortical bone dynamics and*658 structure after lactation in established breeder rats. Anat Rec A Discov Mol Cell Evol
 659 Biol, 2004. **276**(2): p. 143-9.
- Brembeck, P., et al., Changes in cortical volumetric bone mineral density and thickness, and trabecular thickness in lactating women postpartum. J Clin Endocrinol Metab, 2015. 100(2): p. 535-43.

- Bjornerem, A., et al., Irreversible Deterioration of Cortical and Trabecular
 Microstructure Associated With Breastfeeding. J Bone Miner Res, 2017. 32(4): p. 681-665
- M, O.B., A. Prentice, and K. Ward, Pregnancy-Related Bone Mineral and
 Microarchitecture Changes in Women Aged 30 to 45 Years. J Bone Miner Res, 2020.
 35(7): p. 1253-1262.
- Liu, X.S., et al., Site-specific changes in bone microarchitecture, mineralization, and stiffness during lactation and after weaning in mice. J Bone Miner Res, 2012. **27**(4): p. 865-75.
- de Bakker, C.M., et al., Adaptations in the Microarchitecture and Load Distribution of
 Maternal Cortical and Trabecular Bone in Response to Multiple Reproductive Cycles in
 Rats. J Bone Miner Res, 2017. 32(5): p. 1014-1026.
- de Bakker, C.M.J., et al., Reproduction Differentially Affects Trabecular Bone Depending on Its Mechanical Versus Metabolic Role. J Biomech Eng, 2017. 139(11).
- Vajda, E.G., B.M. Bowman, and S.C. Miller, Cancellous and cortical bone mechanical properties and tissue dynamics during pregnancy, lactation, and postlactation in the rat. Biol Reprod, 2001. **65**(3): p. 689-95.
- Gillies, B.R., et al., Absence of Calcitriol Causes Increased Lactational Bone Loss and
 Lower Milk Calcium but Does Not Impair Post-lactation Bone Recovery in Cyp27b1 Null
 Mice. J Bone Miner Res, 2018. 33(1): p. 16-26.
- 683 26. Physical Activity and Exercise During Pregnancy and the Postpartum Period: ACOG
 684 Committee Opinion, Number 804. Obstet Gynecol, 2020. 135(4): p. e178-e188.
- Lovelady, C.A., et al., Effect of exercise training on loss of bone mineral density during lactation. Med Sci Sports Exerc, 2009. **41**(10): p. 1902-7.
- To, W.W. and M.W. Wong, *Bone mineral density changes during pregnancy in actively exercising women as measured by quantitative ultrasound.* Arch Gynecol Obstet, 2012. **286**(2): p. 357-63.
- Little, K.D. and J.F. Clapp, 3rd, Self-selected recreational exercise has no impact on
 early postpartum lactation-induced bone loss. Med Sci Sports Exerc, 1998. 30(6): p. 831 6.
- 693 30. Dimov, M., J. Khoury, and R. Tsang, *Bone mineral loss during pregnancy: is tennis protective?* J Phys Act Health, 2010. **7**(2): p. 239-45.
- Rosa, B.V., et al., Voluntary exercise in pregnant rats improves post-lactation maternal bone parameters but does not affect offspring outcomes in early life. J Musculoskelet Neuronal Interact, 2012. 12(4): p. 199-208.
- 698 32. Bonewald, L.F., *The amazing osteocyte*. J Bone Miner Res, 2011. **26**(2): p. 229-38.
- 699 33. Klein-Nulend, J., et al., *Mechanosensation and transduction in osteocytes*. Bone, 2013. 54(2): p. 182-90.
- 701 34. Wang, L., Solute Transport in the Bone Lacunar-Canalicular System (LCS). Curr Osteoporos Rep, 2018. **16**(1): p. 32-41.
- 703 35. Qing, H., et al., Demonstration of osteocytic perilacunar/canalicular remodeling in mice during lactation. J Bone Miner Res, 2012. **27**(5): p. 1018-29.
- 705 36. Kaya, S., et al., Lactation-Induced Changes in the Volume of Osteocyte Lacunar-706 Canalicular Space Alter Mechanical Properties in Cortical Bone Tissue. J Bone Miner 707 Res, 2017. **32**(4): p. 688-697.

- Jahn, K., et al., Osteocytes Acidify Their Microenvironment in Response to PTHrP In
 Vitro and in Lactating Mice In Vivo. J Bone Miner Res, 2017. 32(8): p. 1761-1772.
- Tang, S.Y., et al., *Matrix metalloproteinase-13 is required for osteocytic perilacunar remodeling and maintains bone fracture resistance.* J Bone Miner Res, 2012. **27**(9): p. 1936-50.
- 713 39. Lotinun, S., et al., *Cathepsin K-deficient osteocytes prevent lactation-induced bone loss* and parathyroid hormone suppression. J Clin Invest, 2019. **129**: p. 3058-3071.
- 715 40. Dole, N.S., et al., TGFbeta Regulation of Perilacunar/Canalicular Remodeling Is Sexually Dimorphic. J Bone Miner Res, 2020.
- 717 41. Kegelman, C.D., et al., *YAP and TAZ Mediate Osteocyte Perilacunar/Canalicular Remodeling*. J Bone Miner Res, 2020. **35**(1): p. 196-210.
- Lai, X., et al., Lactation alters fluid flow and solute transport in maternal skeleton: a
 multiscale modeling study on the effects of microstructural change and loading
 frequency. Submitted to Bone: Mechanobiology Special Issue, 2021.
- Wang, B., et al., Perlecan-containing pericellular matrix regulates solute transport and mechanosensing within the osteocyte lacunar-canalicular system. J Bone Miner Res, 2014. **29**(4): p. 878-91.
- Fritton, J.C., et al., Loading induces site-specific increases in mineral content assessed by microcomputed tomography of the mouse tibia. Bone, 2005. **36**(6): p. 1030-8.
- Main, R.P., et al., Murine Axial Compression Tibial Loading Model to Study Bone
 Mechanobiology: Implementing the Model and Reporting Results. J Orthop Res, 2020.
 38(2): p. 233-252.
- Lan, S., et al., 3D image registration is critical to ensure accurate detection of longitudinal changes in trabecular bone density, microstructure, and stiffness measurements in rat tibiae by in vivo microcomputed tomography (muCT). Bone, 2013.
 56(1): p. 83-90.
- 734 47. Johnson, H.J., M. McCormick, and L. Ibanez, *The itk software guide third edition updated for itk version 4.5.* Insight Software Consortium, Tech. rep, 2013.
- Houxsein, M.L., et al., Guidelines for assessment of bone microstructure in rodents using micro-computed tomography. J Bone Miner Res, 2010. **25**(7): p. 1468-86.
- 738 49. Dempster, D.W., et al., Standardized nomenclature, symbols, and units for bone 739 histomorphometry: a 2012 update of the report of the ASBMR Histomorphometry 740 Nomenclature Committee. J Bone Miner Res, 2013. **28**(1): p. 2-17.
- 741 50. Ploton, D., et al., *Improvement in the staining and in the visualization of the argyrophilic* 742 proteins of the nucleolar organizer region at the optical level. Histochem J, 1986. **18**(1): 743 p. 5-14.
- Dole, N.S., et al., Osteocyte-Intrinsic TGF-beta Signaling Regulates Bone Quality
 through Perilacunar/Canalicular Remodeling. Cell Rep, 2017. 21(9): p. 2585-2596.
- 746 52. Milgrom, C., et al., *A home exercise program for tibial bone strengthening based on in vivo strain measurements*. Am J Phys Med Rehabil, 2001. **80**(6): p. 433-8.
- Vainionpaa, A., et al., *Intensity of exercise is associated with bone density change in premenopausal women.* Osteoporos Int, 2006. **17**(3): p. 455-63.
- 750 54. Hemmatian, H., et al., Mechanical Loading Differentially Affects Osteocytes in Fibulae
 751 from Lactating Mice Compared to Osteocytes in Virgin Mice: Possible Role for Lacuna
 752 Size. Calcif Tissue Int, 2018. 103(6): p. 675-685.

- 753 55. Ardeshirpour, L., et al., *Increased PTHrP and decreased estrogens alter bone turnover*754 *but do not reproduce the full effects of lactation on the skeleton.* Endocrinology, 2010.
 755 **151**(12): p. 5591-601.
- 756 56. Bornstein, S., et al., *FGF-21 and skeletal remodeling during and after lactation in C57BL/6J mice*. Endocrinology, 2014. **155**(9): p. 3516-26.
- 758 57. de Bakker, C.M.J., et al., *Effects of reproduction on sexual dimorphisms in rat bone mechanics*. J Biomech, 2018. 77: p. 40-47.
- 760 58. Ross, R.D., M.J. Meagher, and D.R. Sumner, Calcium restriction during lactation has
 761 minimal effects on post-weaning mineral metabolism and bone recovery. J Bone Miner
 762 Metab, 2019. 37(4): p. 648-657.
- 763 59. Nango, N., et al., *Osteocyte-directed bone demineralization along canaliculi*. Bone, 2016. **84**: p. 279-288.
- Wittig, N.K., et al., No Signature of Osteocytic Osteolysis in Cortical Bone from
 Lactating NMRI Mice. Calcif Tissue Int, 2019. 105(3): p. 308-315.
- 767 61. Tsourdi, E., et al., *Physiological and pathological osteocytic osteolysis*. J Musculoskelet Neuronal Interact, 2018. **18**(3): p. 292-303.
- 769 62. Fritton, S.P. and S. Weinbaum, *Fluid and Solute Transport in Bone: Flow-Induced Mechanotransduction*. Annu Rev Fluid Mech, 2009. **41**: p. 347-374.
- 771 63. Price, C., et al., Real-time measurement of solute transport within the lacunar-772 canalicular system of mechanically loaded bone: direct evidence for load-induced fluid 773 flow. J Bone Miner Res, 2011. **26**(2): p. 277-85.
- Weinbaum, S., S.C. Cowin, and Y. Zeng, A model for the excitation of osteocytes by mechanical loading-induced bone fluid shear stresses. J Biomech, 1994. **27**(3): p. 339-60.
- Wang, B., et al., Quantifying load-induced solute transport and solute-matrix interaction within the osteocyte lacunar-canalicular system. J Bone Miner Res, 2013. **28**(5): p. 1075-86.
- 780 66. Yee, C.S., et al., *Investigating Osteocytic Perilacunar/Canalicular Remodeling*. Curr Osteoporos Rep, 2019. **17**(4): p. 157-168.
- 782 67. Lai, X., et al., *The dependences of osteocyte network on bone compartment, age, and disease.* Bone Res, 2015. **3**.
- Hemmatian, H., et al., *Aging, Osteocytes, and Mechanotransduction*. Curr Osteoporos Rep, 2017. **15**(5): p. 401-411.
- 786 69. Lynch, M.E., et al., *Tibial compression is anabolic in the adult mouse skeleton despite reduced responsiveness with aging.* Bone, 2011. **49**(3): p. 439-46.
- 788 70. Pathirathna, M.L., et al., Effects of Physical Activity During Pregnancy on Neonatal Birth Weight. Sci Rep, 2019. **9**(1): p. 6000.
- 790 71. Nguyen, P.T.H., et al., *Physical Activity During Pregnancy is Associated with Improved*791 *Breastfeeding Outcomes: A Prospective Cohort Study.* Int J Environ Res Public Health,
 792 2019. **16**(10).
- 793 72. Larson-Meyer, D.E., *Effect of postpartum exercise on mothers and their offspring: a review of the literature.* Obes Res, 2002. **10**(8): p. 841-53.
- 795 73. Torcasio, A., et al., 3D characterization of bone strains in the rat tibia loading model.
 796 Biomech Model Mechanobiol, 2012. 11(3-4): p. 403-10.

74. Mazur, C. and T. Alliston. Evidence for site-specific mechanoregulation of osteocyte 798 perilacunar/canalicular remodeling. in American Society of Bone and Mineral Research 799 Annual Meeting. 2020.